



Soft Matter

Accepted Manuscript

This article can be cited before page numbers have been issued, to do this please use: K. Chakraborty, W. Shinoda and S. Loverde, *Soft Matter*, 2020, DOI: 10.1039/C9SM02165E.



This is an Accepted Manuscript, which has been through the Royal Society of Chemistry peer review process and has been accepted for publication.

Accepted Manuscripts are published online shortly after acceptance, before technical editing, formatting and proof reading. Using this free service, authors can make their results available to the community, in citable form, before we publish the edited article. We will replace this Accepted Manuscript with the edited and formatted Advance Article as soon as it is available.

You can find more information about Accepted Manuscripts in the <u>Information for Authors</u>.

Please note that technical editing may introduce minor changes to the text and/or graphics, which may alter content. The journal's standard <u>Terms & Conditions</u> and the <u>Ethical guidelines</u> still apply. In no event shall the Royal Society of Chemistry be held responsible for any errors or omissions in this Accepted Manuscript or any consequences arising from the use of any information it contains.





Journal Name

ARTICLE

Molecular Simulation of the Shape Deformation of a Polymersome

Kaushik Chakraborty^a, Wataru Shinoda^b, Sharon M. Loverde^{a,c,d,e,*}

28

29

Received 00th January 20xx, Accepted 00th January 20xx

DOI: 10.1039/x0xx00000x

www.rsc.org/

Vesicles composed of diblock copolymers, or polymersomes, have proven to possess numerous applications ranging from drug delivery to catalytically driven nano-motors. The shape of a polymersome can be responsive to external stimuli, such as light or solvent. Molecular dynamics simulations reveal that the shape change upon the contraction of the inner volume of a polymersome vesicle occurs in two separate regimes—a stretching regime and a bending regime. The barrier is shown to be dependent on the solvent environment. These results suggest that tailoring the bending modulus of polymer membranes can be used as a design methodology to engineer new stimuli-responsive vesicles.

A. Introduction

Published on 04 March 2020. Downloaded by RSC Internal on 3/5/2020 10:14:04 AM

5

10

11

12

13

14

15

16

17

18

19

20

21

22

23

24

25

"Polymersomes" are diblock copolymer membranes that form 39 vesicle shape in solution 1, 2. Due to their high molecular weight polymer vesicles as compared with phospholipid vesicles possess higher mechanical rigidity and a lower water permeability 3. Fo example, phospholipid membranes can possess a bending rigidit approximately in the range of 0.2–1.3 $\times 10^{-19}$ J ($\sim 5-30 \text{ k}_B$ T) while diblock copolymer membranes have a bending rigidity that can range from approximately 1.3–20.0 $\times 10^{-19}$ J (~30 – 500 k_BT) The inherent hydrophobicity and thickness of polymer membrana (~4-15 nm) as compared with phospholipid membranes (~2-4 กตั imparts a selective permeability to polymer membranes. This solve selectivity can be harnessed to engineer and fine-tune membranes and polymersomes that are responsive to solvent concentration \overline{t} form unique shapes. Stimuli-responsive polymersomes have diver materials applications as nanocarriers $^{6,\,7}$, nanoreactors 8 , and even_{7} as biomimetic systems 9, 10.

equilibrium **Besides** the spherical geometi polymersomes often deform to form a range of shapes including disco-cytes, dumbells, pear-shaped vesicles, and stomatocytes dependent on the surrounding environment ¹¹. These shape transformations are generally induced by a change in the osmot conditions surrounding a membrane, leading to a balance between the change in internal concentration of the membrane (osmog) pressure) and its bending energy 12. The free energy of fluid, not crystalline membranes in vesicular shapes has contributions due to the bending rigidity, κ_{G} , and the Gaussian bending rigidity, κ_{G} , plus $\xi \overline{\chi}$

osmotic pressure difference inside and outside the membranes, as well as the surface tension 12, 13 as follows:

$$F = \int (f_C + \gamma) dA + \Delta p \int dV$$

 $F=\int (f_C+\gamma)dA+\Delta p\int dV$ where $f_c=\frac{\kappa_c}{2}(2H+c_o)^2+\kappa_G K$ and c_o is the spontaneous curvature, H is the mean curvature, and K is the Gaussian curvature of the membrane. The equilibrium shape of a spherical bilayer was shown by Ou-Yang and Helfrich¹³ to satisfy the following equation:

 $\Delta p - 2\gamma H + \kappa (2H + c_0)(2H^2 - c_0 H - 2K) + 2\kappa \nabla^2 H = 0$ The threshold pressure for instability was shown to be $\Delta p_C \propto \kappa/R^3$. where R is the radius of the vesicle. The elastic properties of polymersomes, such as the membrane bending and area expansion moduli can be tuned based on the unique diblock copolymer compositions, with well-known scaling relations 14. For example, the area expansion modulus, KA, for block copolymer membranes is determined by the strength of the interfacial tension, $K_A \sim 4\gamma$, which varies with respect to polymer chemistry and environment 14, 15. The interfacial tension and thus the area elastic modulus can be tuned through cross-linking one of the components 16 or blending the membrane with an additional copolymer or surfactant of different molecular weight ^{10, 17}. The bending modulus has been experimentally shown to scale with the thickness of the membrane, $\kappa \sim K_A d^2$ 5.

Common copolymer chemistries that form polymersomes include copolymers such as polythethylene oxide—polystyrene (PEO-PS) and PEO-polyethylethylene (PEE) 2. In addition, polyester based copolymers with biodegradable hydrophobic segments such as poly caprolactone (PCL) and polylactic acid (PLA) have also been shown to form these functional assembled membranes, oftentimes used with blends of inert copolymers such as PEO-polybutadiene (PEO-PBD) to modulate degradation and release profiles ³. While morphologies and characteristics of PS-based vesicles have previously been characterized in great detail 18, 19, recently, there has been a revived interest in glassy polymersomes 20. For example, as shown by Kim et al 21, dependent on the water and solvent concentration inside and outside of the membrane, these vesicles can be inflated or deflated as the osmotic pressure difference varies. Furthermore, Wilson et al 8, 11, 22-24 showed that during dialysis against water, after preparing a PEO-PS polymersome in a mixture of water and organic solvents, induces an osmotic pressure difference

56

57

a. Department of Chemistry, College of Staten Island, The City University of New York, 2800 Victory Boulevard, Staten Island, New York, 10314 U.S.A.

b. Department of Materials Chemistry, Nagoya University, Furo-cho, Chikusa-ku, Nagoya 464-8603, Japan

c. Ph.D. Program in Chemistry. The Graduate Center of the City University of New York, New York, NY, 10016 U.S.A.

^{d.} Ph.D. Program in Biochemistry, The Graduate Center of the City University of New York, New York, NY, 10016, U.S.A.

e. Ph.D. Program in Physics. The Graduate Center of the City University of New York. New York, NY, 10016 U.S.A.

it Matter Accepted mar

View Article Online

DOI: 10.1039/C9SM02165E

53

57

59

3

5

6

ARTICLE Journal Name

between inside and outside of the polymersome membrane and transforms the spherical geometry to a stomatocyte. In particular, the formation of the stomatocyte occurs in a region given by a range of reduced volumes and reduced areas of the inner compartment of the polymersome as compared to the ideal spherical shape ^{12, 25} does to rapid outward diffusion of the organic solvent during dialysis. The degree of shape deformation is found to be correlated to the amount of cosolvent in the mixture ²¹. Before reaching the stomatocyte conformation, the polymersome forms a series of non-spherical structures ranging from prolate to disk ¹¹.

While continuum models have been long been utilized $\frac{70}{100}$ predict non-spherical topologies of fluid membranes and vesicles 1977 26 , the use of particle-based methodologies including such method 38 as Monte Carlo, Dissipative Particle Dynamics (DPD), and molecular dynamics to characterize the shape transformation and/or stability of polymer vesicles are ongoing ^{27, 28}. One constraint in utilizing particle-based models to predict the materials properties of polymer assemblies is the accuracy and thus the predictive power of the polymer force field ²⁹. Computational models of PS and additive ²⁹ possess a long history 30-32 with PS increasingly well-studied by bo80 all-atomistic 33 and CG molecular dynamics simulations 34. Numero 81 molecular-based models for PS have been developed, utilizing bo82 structural 34 and thermodynamic 35 mapping methodologies 36. We have designed a CG model for PS based on all-atomistic simulations 37 that is compatible with the CG model for PEO developed by Shinoda et al ³⁶. The CG water model is also developed by Shino 85 et al ³⁶. The PS model was first characterized to show the correct scaling behavior for the radius of gyration of the polymer as \bar{o} function of molecular weight in a poor solvent (water) 37. Next, the PEO-PS force field was utilized to characterize the nature of glasaγ worm-like and spherical micelles³⁸. Herein, we extend this coare grain force field for PEO-PS diblock copolymers of certain amphiphidio fraction to characterize the elastic properties (K_A and κ) of PEO- $\bar{8}$ § diblock copolymer membranes. We show that PEO-PS membranes exhibit an expected K_A and κ , consistent with experimental measurements. We demonstrate that expected $K_{\mathbf{A}}$ is independent of the length of the copolymer, for low copolymer weights atog certain hydrophilic fraction. For the shortest copolymer, vigo characterize and predict κ and show that this rigidity decreases with incorporation of a model hydrophobic solvent. We next utilize ដាំ model to characterize perturbations to the structure of nearly 0.05micron-sized polymersomes and explore the process of shape deformation. We find two different regimes in the shape chang \bar{q} these model PEO-PS vesicles, the first dominated by stretching of \bar{t} membrane and reorientation of the polymer chains, the second regime dominated by the splaying of the polymer chains.

We develop a simple algorithm to accelerate the process of diffusion of the solvent from the inner compartment by gradually moving water from inside of the polymersome to outside in multiple cycles. After each cycle the simulation is run long enough for the polymersome shape to equilibrate, approximately 50 ns. The inner volume of the polymersome shape changes upon removal of the water, and, as a result, the polymer vesicle forms a non-spherical shape. The shape change undergoes two major structural rearrangements of the polymer bilayer membrane. First, the hydrophobic core stretches longitudinally. Next, this is followed by the bending and crumpling of the membrane inward. The free energy analysis of the shape change of the polymersome calculated with Umbrella Sampling 39 further reveals that the stretching and the bending regimes of PEO-PS membrane are separated by a fighter energy barrier on the order of 20 kcal/mol.

B. Methods

Due to the large system size and longer time scales involved in these PEO-PS membrane and polymersomes, coarse-grained (CG) based molecular dynamics simulation (CG-MD) is the ideal methodology to study the self-assembly of di-block co-polymers like PEO-PS. CG models have been routinely used to study self-assembly of different biological, as well as synthetic soft materials, including polymers, peptides, proteins, and membranes in science and engineering 40-45. The CG parameters for PS are developed by Drenscko et al. 37, based on a Shinoda-DeVane-Klein (SDK) 46 coarse-graining approach. The parameters for PEO and water are developed by the Klein group 44, ^{47, 48}. Intra-molecular interactions in the SDK model are calculated via harmonic potentials given by $V_{
m bond}(r) = K_b(r-r_0)^2$ and $V_{\rm angle}(\theta) = K_a(\theta - \theta_0)^2$, respectively. Here, K_b and r_0 are the equilibrium force constant and distance for bond stretch, and K_{a} and $heta_0$ are the equilibrium bending force constant and equilibrium value for angles. Non-bonded interactions are set by a pair-wise additive potential based on the Lennard-Jones (LJ) potential: $U_{LJ9-6}=% \left(\frac{1}{2}\right) \left($ $(27/4)\varepsilon\{(\sigma/r)^9 - (\sigma/r)^6\}$ or $U_{L/12-4} = (3\sqrt{3}/2)\varepsilon\{(\sigma/r)^{12} - (\sigma/r)^{12}\}$ $r)^4$ 49. Cross-interactions between the PEO and PS are estimated assuming a combination rule between the PEG-CG bead, i, and PS CG group, j, where $\varepsilon_{ij}=\left(\varepsilon_{ii}\varepsilon_{jj}\right)^{1/2}$ and $\sigma_{ij}=(\sigma_{ii}+\sigma_{jj})/2$. We have previously tested these CG parameters for PEO-PS worm micelles³⁸. Here, we usie a model weakly hydrophobic bead to mimic the fluidizing effect of solvent on the shape transformation of a polymersome. The solvent LJ parameters, both ε and σ , are the same as the interfacial bead of the PEO-PS polymer, as defined in SI Table

To test this model further, four different CG bilayer membranes with polymer chain lengths PEO₃-PS₁₅, PEO₁₁-PS₄₃, PEO₁₆-PS₆₄, and PEO₂₂-PS₈₆ are simulated in an aqueous medium. All of the bilayers contain 100 polymers and 100,000 water molecules. The total number of beads in each system varies between 150,000-200,000. 100 ns trajectories are generated for each bilayer system with the time step of 10 fs. All simulations are performed under NPT conditions at 300 K and 1 atm using LAMMPS 50 using Nose-Hoover thermostat51 using the equations of motion from Shinoda et al 52 and Parrinello-Rahman barostat 53 and the equations of motion of Martyna et al 54. In addition to the bilayer membranes, we also equilibrated two small polymersomes with polymer chain lengths PEO₃-PS₁₅ and PEO₁₁-PS₄₃. Each system contains 1300 polymers and 400,000 water molecules. The total number of CG beads for PEO₃-PS₁₅ and PEO₁₁-PS₄₃ polymersomes are around 500,000 and 700,000 respectively. Finally, a large polymersome with diameter around 40 nm is setup. The system contains 10,300 PEO₃-PS₁₅ polymers and 1,090,000 water molecules. Altogether it has 1,759,500 beads. 100 ns trajectories are generated for each polymersome under NPT conditions.

Umbrella Sampling.

To construct the free energy profile for the shape change of the PEO-PS polymersome due to contraction of inner compartment, we used umbrella sampling (US) techniques 55 for efficient sampling. The reaction coordinate for the US is the radius of gyration of the inner leaflet $(r_{g_{\,i}})$ of the polymersome. A harmonic potential, $\frac{1}{2}k(r_{g_{\,i}}-r_{g_{\,i}}^{0})^2$, was employed during simulation. Here, the force constant $k=2\ kcalmol^{-1} \mathring{\rm A}^{-2}$ and $r_{g_{\,i}}^{0}$ is the reference radius of gyration of the inner leaflet. The initial configuration of 20 different cycles are

2

6

7

8

9

20

21

22

23

24

25

26

27

28

29

30

31

32

33

34

35

Journal Name ARTICLE

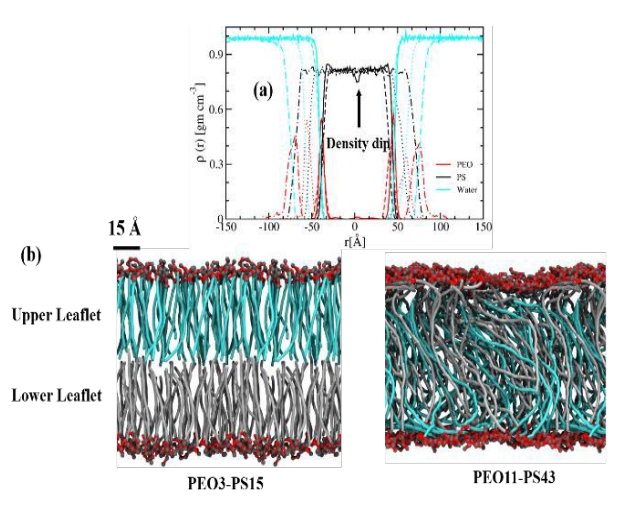


Fig 1. (a) Density profile of PEO₃-PS₁₅ (solid line), PEO₁₁-PS₄₃ (dashed line), PEO₁₆-PS₆₄ (dotted line), and PEO₂₂-PS₈₆ (dot-dashed line) membranes. Hydrophilic fraction is constant. (b) Snapshot after 100 ns simulation of a CG'ed model of a PEO-PS diblock copolymer membrane, specifically PEO₃-PS₁₅ and PEO₁₁-PS₄₃. PEO is grey and red, PS is cyan (upper leaflet) and silver (lower leaflet).

chosen as 20 individual reference points for US simulations. For eads window we performed 30 ns simulation. Finally, to obtain the potential of mean force (PMF) as a function of $r_{\!g_i}$ we used the weighted histogram analysis method (WHAM) 56,57. 48

C. Results and Discussion

Properties of Membrane.

To begin with, to validate the PEO-PS force field, we utilize long-time. coarse grain molecular dynamics (CG-MD) to characterize structural and mechanical properties of PEO-PS bilayers with increasing, copolymer chain lengths at the same hydrophilic fraction. Due to the slow dynamics of the long PS chains, as investigated and characterized for PEO-PS spherical and cylindrical micelles ⁵⁸, we do not characterize the self-assembly of bilayers at this time. However we note that approaches such as MC with implicit solvent could $6e^{-1}$ an alternative approach to equilibrate these systems ⁵⁹. We simula 62 four different CG bilayer membranes with varying copolymer changes lengths PEO₃-PS₁₅, PEO₁₁-PS₄₃, PEO₁₆-PS₆₄, and PEO₂₂-PS₈₆, compos 624 by EO_m -PS_n, where $m = N_{EO}$ and $n = N_{PS}$ are the indicated number of monomers. Bilayer membranes were made, keeping constant the hydrophilic monomer fraction, f_{EO} ~. 1, where $f_{EO}=m_{EO}N_{EO}/$ $(m_{EO}N_{EO} + m_{PS}N_{PS})$, consistent with the vesicle phase.

Structural Properties of Membrane.

Along with water, the average density profiles of both PEO and PS along the normal to the bilayer plane are highlighted in Figure 1(a). Irrespective of polymer chain length, a narrow density profile of PEO suggests a sharp interface between the hydrophobic PS core of the membrane and hydrophilic PEO. In addition to the interface, the profile further reveals a density dip near the center of the bilayers for the shortest polymer chain length (PEO₃-PS₁₅). A similar density dip was also reported previously 60 between the two leaflets of a lipid bilayer as well as a polymer membrane with small chain lengths. As the membrane becomes thicker with increasing polymer chain length, the density dip disappears and a localized density of PS near

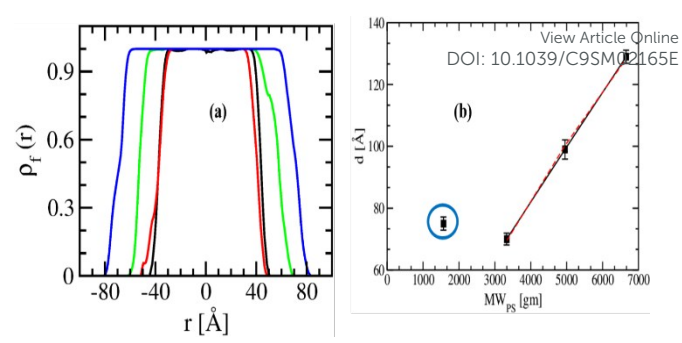


Fig 2. (a) Variation of density fraction of PS $(
ho_f)$ form the center of PEO-PS membrane with four different chain lengths. Black line for PEO₃-PS₁₅, red for PEO₁₁-PS₄₃, green for PEO₁₆-PS₆₄, and blue for PEO₂₂-PS₈₆. (b) Scaling of the membrane core thickness, d, as a function of MW_{phob}, $d \sim MW_{phob}^{0.589}$.

the center with a plateau value of 0.8 g/cm³ is observed. This again agrees well with previous simulation studies 61, 62 of diblock copolymer membranes. In Figure 1(b), we present the final snapshots of PEO₃-PS₁₅ and PEO₁₁-PS₄₃ membranes after 100 ns. The two leaflets of each membrane are shown in different colors. In agreement with the density dip, the snapshot depicts very little or nearly no overlap between the two leaflets of the PEO₃-PS₁₅ membrane. In contrast, for the PEO₁₁-PS₄₃ membrane, the PS polymer chain ends interpenetrate within the hydrophobic core. Hence, due to the overlap of the leaflets, the density dip disappears for long copolymer chain lengths.

Scaling With Molecular Weight.

49

50

51

52

The width of the membrane also depends on the melting of its two leaflets. Mean field arguments of the strong segregation limit (SSL) predict the width of the hydrophobic core, $d \sim N_h^{2/3}$, where N_h is the length of the hydrophobic polymer in the bilayer/vesicle phase. For fully stretched chains, $d \sim N_h$, while for ideal chains, $d \sim N_h^{1/2}$. Experimentally, for the case of PEO-PBD, as well as computationally via mesoscopic simulation techniques 61, for the case of PEO-PEE, the scaling has been found to be close to the ideal random chain 14. To compute the width of the hydrophobic core, we calculate the density fraction of PS $(
ho_f)$ as a function of distance from the central core region. ho_f is defined as $rac{
ho_{PS}}{
ho_{PS}+
ho_{PEO}}$. Variation of ho_f against normal to the bilayer plane are highlighted in **Figure 2(a)**. Any regions with ho_f greater than 0.8 are considered as a part of the membrane hydrophobic core. As molecular weight of the PS (MW_{phob}), is

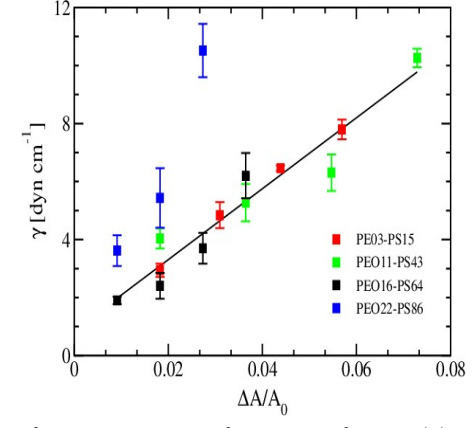


Fig 3. Surface tension vs area of expansion of PEO-PS bilayers. The slope leads to an estimate of the area elastic modulus, KA, of approximately 125 dyne/cm. Each simulation was run for 20.0 ns.

Soft Matter Accepted Manuscript

2

3

4

5

6 7

8

9

10

11

12

13 14

15

16

17

18

19

20

21

22

23

24

25

26

27

28

29

30

31

33

34

35

36

37

38

39

40

41

42

43

44

45

46

47

48

49

50

ARTICLE Journal Name

proportional to the length of the hydrophobic polymer, N_h in Figure 2 **2**(b), we have shown the variation d for a range of MW_{phob}. **T58** thickness of the bilayer for higher molecular weights is given by tb4 relation, $d \sim MW_{phob}^{0.589}$, which is close to the ideal random chabs limit. This is also consistent with previous experiments ¹⁴ and rece**56** simulation studies 62 for PEO- PBD membranes. However, for the lowest molecular weight (PEO₃-PS₁₅), the width of the hydrophobic core deviates from the ideal random chain limit. For the lower molecular weights, less entropic force is needed to stretch the chains, which causes them to more tightly pack, as they deviate from the ideal configuration of the random chain. This naturally leads to less interpenetration as the chains approach the brush limit.

fitting the data points for individual membranes. While KA is not predicted to be dependent on the molecular weight of the polymer. here initial results suggest an increase at higher diblock copolymer lengths, which is contrary to previous findings and is likely an artifact due to limited sampling, especially considering the long molecular

Mechanical Properties

To study the elastic properties of the bilayer, we next calculate the membrane area elasticity for PEO-PS diblocks for a range of molecular weights. Considering similar values of Hildebrand solubility coefficients for PS and polybutadiene (PBD), the interfacial tension between PEO and PS, $\gamma_{\text{PEO-PS}}$ is expected to be similar to PEO and PBD, $\gamma_{PEO-PDB} = 26$ mN/m. From the interfacial tension one can estimate the area elastic modulus, $K_A = 4\gamma_{interface} = 102$ mN/m, which is predicted to be independent of the molecular weight of the polymer. We make a simple computational estimate of KA for a PEO-PS bilayer membrane from the slope of the tension (γ) vs. area

Chain Length	K _A [dyne cm- ¹]	A ₀ [Å ²]
PEO ₃ -PS ₁₅	129.6 (±2.3)	76.2 (± 0.2)
PEO ₁₁ -PS ₄₃	118.1 (±5.1)	241.3 (± 0.8)
PEO ₁₆ -PS ₆₄	122.2 (±4.5)	253.7 (± 0.9)
PEO ₂₂ -PS ₈₆	378.5 (±10.6)	262.1 (± 0.4)

Table 1: Area elastic modulus (KA) and area per polymer (AO) of PEO-PS membranes with varying molecular weight.

expansion, $\Delta A/A$, for a given set of diblock lengths. To do so, we stretch each membrane gradually along the xy-plane from its equilibrium structure (zero surface tension). After each stretching, we equilibrate the membrane for 5 ns followed by a 20 ns production run. The final configuration of each production run is used as the starting configuration for the next simulation of the membrane with increased area. We determine γ by using the formula, $\gamma = \langle (L_z/2) [(P_{zz}$ $-(P_{xx} + P_{yy})/2)$, where P_{ii} is the ij component of the pressure tensor and Lz is the box length along the z-axis. The calculations of y along each of the trajectories have been carried out by averaging over 4 different blocks each with 5 ns duration, using a block averaging approach. The variations of γ due to stretching for all four membranes with different polymer chain lengths are shown in Figure 3. Irrespective of chain length, artificially stretching the membrane shows an increase in surface tension. A close comparison between the membranes further suggests that for the longest chain length (PEO₂₂-PS₈₆), the increment in surface tension with increasing surface area is relatively higher compared to other membranes. Due to higher γ values, to estimate the area average elastic modulus, K_A , we calculate the slope of surface tension vs. area expansion without considering the data for PEO₂₂-PS₈₆. The average K_A is found to be around 125 dyne/cm or 125 mN/m, which is close to the initial theoretical estimate of 102 mN/m. In addition, a $K_A \sim 120$ mN/m has been also reported for polyethylene oxide - polyethylethylene (PEO-PEE) polymersomes. In Table 1 we also present results of estimated K_A 's and equilibrium area per polymer chain A_0 for four different lengths of PEO-PS diblocks. These measurements are performed by Published on 04 March 2020. Downloaded by RSC Internal on 3/5/2020 10:14:04 AM.

3

4

5

6

7

8

9

12

13

14

15

16

17

18

19

20

21

22

23

24

25

26

27

Journal Name ARTICLE

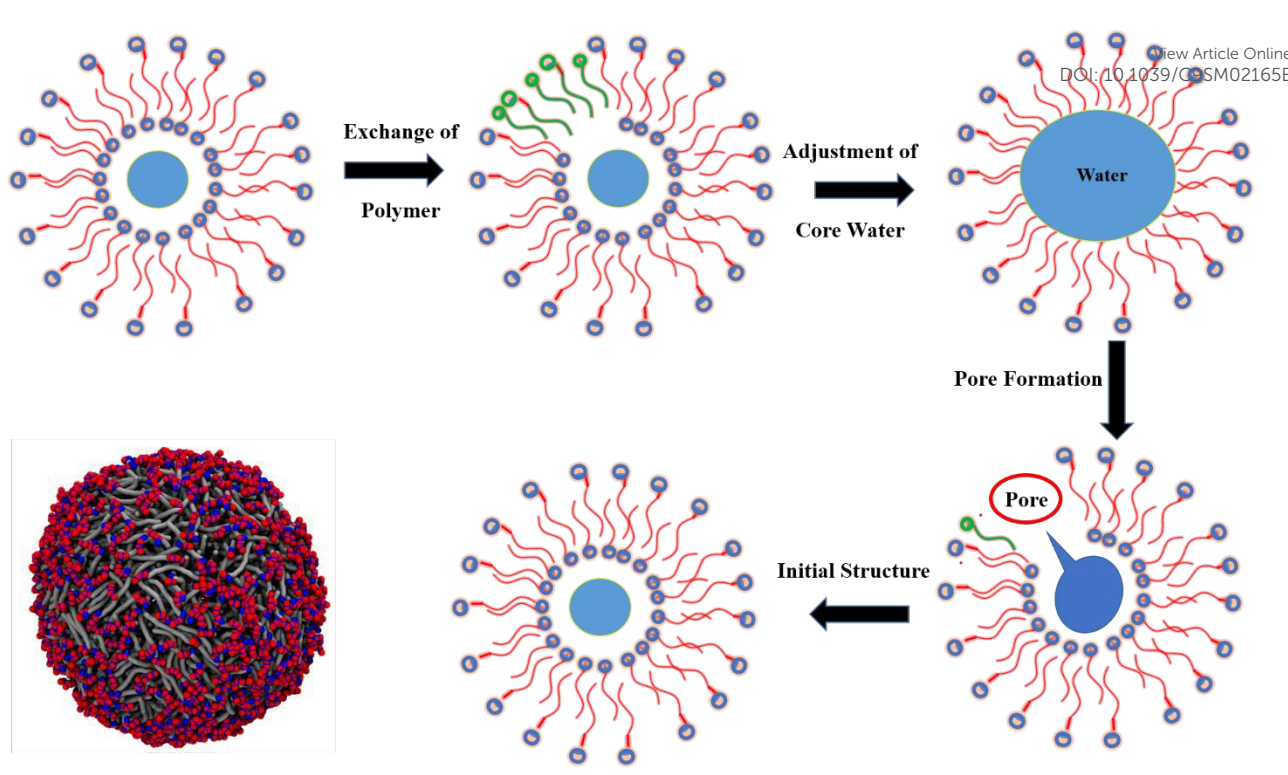


Fig 4. Schematic representations of the four steps to get a well equilibrated preassembled polymersome structure. The first step is the exchange of polymers between the inner and outer leaflets. The second step is the adjustment of water inside the inner core of the polymersome. In the third step, the polymersome adjusts water number inside the polymersome by forming multiple pores. Finally, we find the well-equilibrated starting structure of the polymersome. The blue circles represent the hydrophilic PEO, while the red lines represent the hydrophobic PS.

36

37

weight of the PS. This needs to be further tested. The computation measurements as shown in **Figure 3** are made using one initized membrane conformation, and calculating the interfacial tension for four different initial membrane areas over 20 ns simulation times 1 More accurate measurements and a better calculation of error case be estimated through averaging over several initial membrace conformations, as well as a greater sampling of initial membrace areas.

10 Polymersome Simulations.

After adjusting the polymer distribution within the polymersome, we next vary the number of water molecules inside the polymersome to best approach an equilibrium structure of the polymersome. With a gradual increase in the number of waters, the polymersome adjusts water density inside by forming multiple pores. After conformational relaxation, the pores again disappear and the polymersome radius adjusts accordingly. With further increase of the number of waters inside the polymersome, the structure starts to disintegrate. Details are shown in **Table 2.** After equilibrating the polymersome structure, we continue the simulations for 100 ns.

.1 Preparation of Initial Structure.

Next, we set up three pre-assembled PEO-PS polymersomes structure with two different polymer chain lengths PEO₃-PS₁₅ and PEO₁₁-PS₄₃. For each case six different trials are performed, holding the number of polymers and the initial core radius of the polymersome constant and varying the number of polymers in the inner and outer leaflets, as well as the concentration of water in the center of the polymersome to set up an equilibrium starting conformation. Detailed steps are shown in Figure 4. First, we start with equal number of polymers (650 for small and 5150 for big polymersomes) (based on the surface area of the inner core) in the inner and outer leaflets of the polymersome. As the initial system is not stable, we next gradually move polymers from the inner leaflet to the outer leaflet keeping the total number fixed. Finally, for the small polymersomes, the stable system contains 550 and 7500 polymers in the inner and outer leaflets respectively, and, in the larger polymersome, there are 3700 and 6600 polymers respectively

Table 2. System details for the preparation of initial structure of the larger PEO₃-PS₁₅ polymersome.

Trial	Number of polymers		Number of
	Inner leaflet	Outer leaflet	waters inside
			the
			polymersome
1	5150	5150	100000
2	4650	5650	100000
3	4150	6150	100000
4	3700	6600	100000
5	3700	6600	110000
6	3700	6600	120000
7	3700	6600	130000

We set up two small polymersomes with polymer chain lengths of PEO₃-PS $_{15}$ and PEO $_{11}$ -PS $_{43}$, with diameters of nearly 20 nm and 30 nm

Journal Name

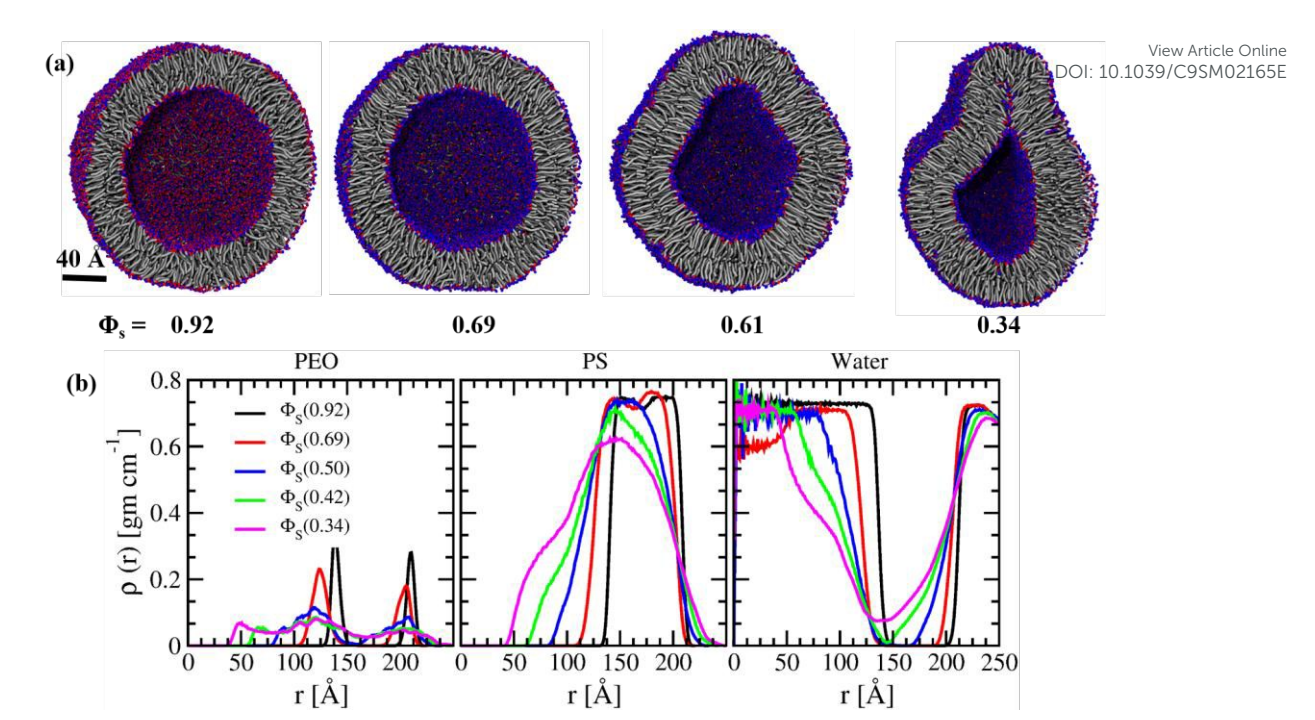


Fig. 5. (a) Final configurations of the PEO₃-PS₁₅ polymersome for four different Φ_s (0.92, 0.69, 0.61 0.34). Φ_s is the fraction of solvent present inside polymersome relative to initial structure. PEO is shown in blue and red and PS in gray. The diameter is approximately 40 nm. When Φ_s drops below 0.6, the polymersome bilayer starts to contract non-spherically. (b) Density profiles of PEO, PS and water from the center of mass of the polymersome.

42

43

44

45

respectively, as shown in SI-1. Each system contains 1300 polyme31 and 400000 water molecules. Finally, a large polymersome wi32 diameter of around 40 nm is simulated for 110 ns (Figure 5). Ti33 system contains 10,300 PEO₃-PS₁₅ polymers and 1,090,000 wat34 molecules. Altogether it has 1,759,500 CG beads. Six trials have be35 performed for each polymersome with varying water number 36 water molecules inside to obtain the optimized for diameter for t36 equilibrium spherical structure. We also test the response of the38 two smaller polymersomes as we shrink the inner compartme329 gradually removing water. Results for the small polymersome a40 also discussed in SI-1 to SI-3.

Polymersome Shape Change

Published on 04 March 2020. Downloaded by RSC Internal on 3/5/2020 10:14:04 AM.

2

3

4

5

6

7

8

9

10

11

12

13

14

15

16

17

18

19

20

21

22

23

24

25

26 27

28

29

30

Next, we computationally mimic the contraction of the inner volume, $\frac{46}{100}$ due to the diffusion of solvent from inside to outside of the polymersome, as in experiments^{11, 23}. The computational process does not correspond to a spontaneous diffusion process. We a artificially accelerating the diffusion of solvent through the membrane. The diffusion of a hydrophobic compound should take place at timescales of seconds to hours, which would allow more time for the vesicle to relax in experiments. We take the final structure of the large 40 nm diameter polymersome after 100 ps simulation time, then randomly select a range of CG solvent beads from 2000 to 10000, from the inner hydrophilic core, place those solvent beads at least 20 Å away from the outer radius of tក្តីខ្ញុំ polymersome and equilibrate for another 30-50 ns until the inner leaflet is equilibrated, and next repeat the cycle. We also test this algorithm for the presence of both CG water and a model CG hydrophobic solvent bead, with parameters characterized by the interfacial bead of the PEO-PS polymer. Twenty cycles (Cycle 1 to

Cycle 20) are performed, for each case. To remove the overlap during the insertion of water at outside the polymersome, we first select a water molecule which is at least 20 Å away from the polymersome and then add a small displacement to its original position. The new position is the updated position of the water molecule that was originally inside the polymersome. Additionally, before gradually increase the time step from 0.01 fs to 10 fs, the system is minimized for 10000 steps. The final snapshots after different cycles for the contraction of the polymersome in CG water are shown in Figure 5(a) and SI-4. Final configurations in presence of 20 % hydrophobic solvent are also incorporated in SI-5. The driving force of the polymersome shape change under osmotic pressure stimuli is the reduction in volume of its inner compartment ^{25, 26}. The density profiles of both polymers and water molecules from the center of the polymer assemblies, as shown in Figure 5 (b), SI-6, and SI-7, characterize the degree of contraction. The contraction of the inner compartment is also evident from the variation of inner core radius (see SI-8). Upon contraction of the vesicle, the density and shape of the PEO and PS significantly shift. Initially when the solvent fraction (Φ_s) is above 0.6 (up to Cycle 6), under the low stress conditions, it contracts symmetrically with an overall spherical structure. Φ_s is the fraction of solvent present inside the polymersome with respect to its equilibrium structure. Transferring more water from inside of the polymersome to outside, contracts the inner core further and the bilayer also starts to bend inward, after which eventually shape of the polymersome becomes non-spherical. The change in spherical symmetry can also be characterized by the variation of the ratio between minimum (I_{min}) and maximum (I_{max}) principle axis of the

1

2

3

4

5

6

7

8 9

10

11

12

13

14

15

16

17

18

19

20

21

22

23

24

25

26

27

28

29

30

Published on 04 March 2020. Downloaded by RSC Internal on 3/5/2020 10:14:04 AM.

Journal Name ARTICLE

43

moment of inertia, I, of the polymersome (Figure 6(a)). Here, I 32 αU Cvcle to the ratio is almost 1 referring to a spherical geometry. Afterward, the value starts to decrease substantially. In comparison, in the case that the solvent is mixed CG water and a model hydrophobic bead, 36 find that the ratio decreases more quickly, indicating the formation? of a non-spherical geometry at earlier cycles. Next, to understand the coupling between the two leaflets of the

polymersome during shape transformation, we compute tHOgyration order parameter (G_r) . G_r is defined as, 42

$$G_r = 1 - \frac{< r_{g_l}(i)>}{< r_{g_l}(0)>}$$

Here $r_{g_1}(0)$ and $r_{g_1}(i)$ are the radius of gyration of the individual leaflets, outer or inner, of the polymersome without and under the osmotic pressure stress conditions respectively. Gr cary vary from 0 to 1. 0 means no contraction of the polymersome will respect to its equilibrium conformation, whereas for fully contractad structures it is 1. Contraction of the individual leaflets of the polymer vesicles is evident from Figure 6(b). It can be further seen that magnitude of the contraction of the two leaflets are significantly different from each other (also see SI 9). Before reaching a plate au region after Φ_s =0.6, the degree of contraction of the inner leaflet relatively higher than the outer leaflet. Such anisotropic contraction is only possible as the hydrophobic core begins to expand. I comparison, in the case that the solvent is mixed CG water and model hydrophobic bead, we find that the inner leaflet contracts to a greater degree in earlier cycles. Figure 6(c) shows the average hydrophobic core width after each cycle. As in the membrane case the density fraction of the hydrophobic core, ρ_f is defined 61 – . Any regions with ho_f greater than 0.8 are considered as 5 $\rho_{PS} + \rho_{PEO}$ part of the hydrophobic core width. The hydrophobic core wid63 increase is only possible since the radius of gyration of the inner co64

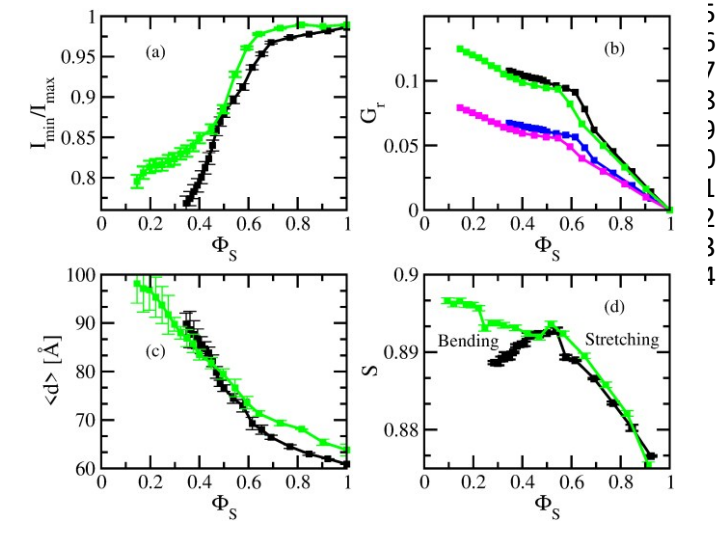


Fig. 6. Variation of average (a) ratio between minimum (I_{min}) and maximum (I_{max}) principle axis (b) gyration order parameter (G_r) (c) width of the hydrophobic core and (d) stretching S of PS counterpart of the PEO-PS polymers as a function of Φ_s . Φ_s is the fraction of solvent present inside the polymersome with respect to its equilibrium structure. The contraction in the presence of only CG water is black, while the contraction in the presence of both CG water and model hydrophobic CG solvent is indicated in green. In (b) the black and blue line correspond to G_r for inner and outer leaflets respectively, while the green and pink line correspond to the G_r for the inner and outer leaflets in the presence of both CG water and CG solvent. Two different regimes, stretching and bending, due to the contraction of the inner compartment of the polymersome emerge.

decreases more quickly than the radius of gyration of the outer core. Indeed, an increase in vesicle thickness of the REQ-RS polymersome under osmotic pressure stress is also found experimentally ²⁴. The equilibrium polymersome vesicle shape balances the membrane bending energy with the line tension of the membrane edge ^{63, 64}. Diffusion of solvent forces the inner compartment of the polymersome to contract. Shrinking decreases the surface area of the polymersome but increases its bending energy. In comparison, in the case that the solvent is mixed CG water and a model hydrophobic bead, we find that the hydrophobic core is thicker, and the increase in thickness continues as cycles continue. By expanding the hydrophobic counterpart, di-block copolymer vesicles minimize the degree of shrinking of the outer leaflet under the osmotic pressure stress to avoid any additional energy cost due to bending.

This increase in core radius can be achieved via stretching of individual polymers. Average stretching S of the PS counterpart of the PEO-PS polymers is shown in Figure 6(d). S is defined as 65

$$s = \frac{x}{I}$$

Here, x and L are the end-to-end distance and contour length of the PS chain respectively. Stretching of the PS chain due to reduced volumes of the polymersome is clearly evident in the beginning of the perturbation to the spherical structure. Importantly, S reaches a maximum at Φ_s =0.6 and afterwards remains constant or decreases very gradually. It correlates nicely with the shape change of the polymersome. Up to Φ_s =0.6 (Cycle 7), due to the stretching of the PS chain, the polymersome contracts symmetrically and maintains a spherical geometry. After the PS chain reaches its maximum stretching limit, after Cycle 7, the polymersome shape is governed by membrane bending and generates non-spherical shapes. Depending on the reduced volume, the presence of two distinct regimes of the polymer membrane response (stretching and bending) is quite clear from all of the four parameters, as shown Figure 6. Hence, in the beginning under low stress conditions, the polymers start to stretch to keep the equilibrium spherical shape of the polymersome via stretching of individual polymers. After a certain threshold limit stretching of the polymers reaches a maximum, bending takes over and the polymersome becomes nonspherical. In comparison, in the case that the solvent is mixed CG water and a model hydrophobic bead, we find that the PS chains stretch to a greater degree in earlier cycles. In addition, the transition to the bending regime occurs at earlier cycles.

Bending Modulus of PEO-PS Bilayer

Soft Matter Accepted Manus

2

3

4

5

6

7

8

9 10

12

13

14

15

16

17

18

19

20

21

22

23

24

25

26

27

28

29

30

31

32

33

34

35

36

ARTICLE Journal Name

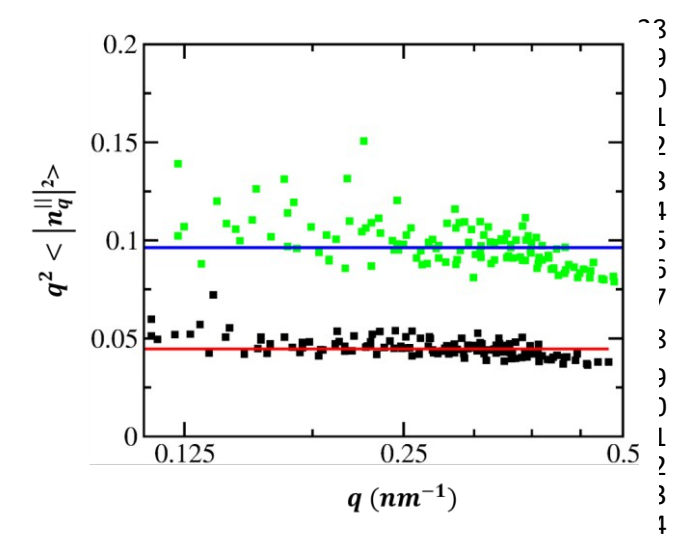


Fig. 7. The spectrum of longitudinal polymer orientation fluctuations $\langle |n^{||}_{q}|^{2} \rangle$ of the PEO-PS bilayer multiplied by q^{2} . The spectrum in the presence of only CG water is black, while the spectrum in the presence of both CG water and model hydrophobic CG solvent is indicated in green.

Considering the relevance of the membrane bending for the shafel transformation of the polymersome under osmotic pressure stimuli, we calculate bending modulus (κ) of the PEO-PS membrane based on the fluctuation spectrum of the polymer orientation. This method has previously been developed and applied to phospholipid membranes ^{66, 67}, but here we apply the method to polymer membranes. In short, κ is related to the fluctuations of polymer orientation ^{67, 68}:

$$\langle |n^{||}_{q}|^{2}\rangle = \frac{K_{B}T}{q^{2}\kappa}$$

Here $n^{||}$ is the longitudinal component of the spectrum of the polymer orientation. The polymer orientation is defined by a vector connecting the two ends of the polymer hydrocarbon chain (PS chain). An additional PEO₃-PS₁₅ membrane with 2000 polymers is simulated for 110 ns in aqueous solution to obtain κ. Figure 7 shows the variation of $n^{||}$ as a function of q. κ is around 22 k_BT . This measurement of κ is similar to what is expected for lipid membranes⁵, but slightly lower than might be expected for polymer membranes. To put this measurement in perspective, the bending rigidity for diblock copolymer membranes have been experimentally reported to range from approximately 20 k_BT up to 500 k_BT , dependent on the specific copolymer chemistry and the molecular weight 5, 14. In comparison, in the case that the solvent is mixed CG water and a model hydrophobic bead (20 %), we find that the bending modulus decreases by approximately 50% to 10 k_BT . The decrease in bending modulus may be related with the decrease in area elastic modulus of the membrane due to the presence of the model hydrophobic solvent. Indeed, previously Bermudez et al.5 found that $K_B = \beta K_A d^2$ where β is a constant and d is the width of the membrane. To check this, we also measure K_A of the PEO₃PS₁₅ membrane in the presence of 20% model hydrophobic solvent. To be consistent with the K_B calculation, we calculate K_A of the larger PEO₃PS₁₅ membrane with 2000 polymers following the same methodology as previously discussed. The variation of γ as a function of surface area of the membrane is shown in SI-10 and the estimated value of K_A from the slope is around 86.2 dyne cm⁻¹. Hence, consistent with K_B , the K_A value also decreases around 33 % in the presence of model hydrophobic solvent.

Free Energy Profile of Polymersome Shape Change View Article Online

Next, we compute the free energy cost of the polymersome going transitioning from the stretching regime to the bending regime. The Potential of Mean Force (PMF) is constructed using US techniques while considering the radius of gyration of the inner leaflet (r_{g_i}) as a reaction co-ordinate. Details can be found in the Supporting Information. As the shape change is happening due to contraction of inner core of the polymersome, the radius of gyration of the inner leaflet is an immediate choice for the reaction coordinate. Besides $r_{\!g_{\,i}}$, the surface area of the inner compartment of the polymersome, local curvature of the bilayer, $\frac{I_{min}}{I_{max}}$ ratio, etc. can also be used as reaction co-ordinates. In general, in US simulations, an external potential is applied to move the system out of the equilibrium. But here, for each window, the starting configuration (initial structure of a particular cycle) is very far from the lowest energy structure for that particular window. As the harmonic potential (H) is applied with respect to the starting configuration, the system moves gradually back to its local minimum with sufficient sampling of the in-between regions. Two distinct regimes, stretching and bending, are observed from Figure 8. It is further found that these two regimes are separated by a high energy barrier of around ~ 20 kcal mol⁻¹. This high energy barrier is consistent with the high bending modulus of the PEO-PS membrane. It is also important to note that, as we are not considering the effect of the hydrophobic

14 15

16

17

18

19

20

21

22

23

24

25

26

27

28 29

Published on 04 March 2020. Downloaded by RSC Internal on 3/5/2020 10:14:04 AM.

Journal Name ARTICLE

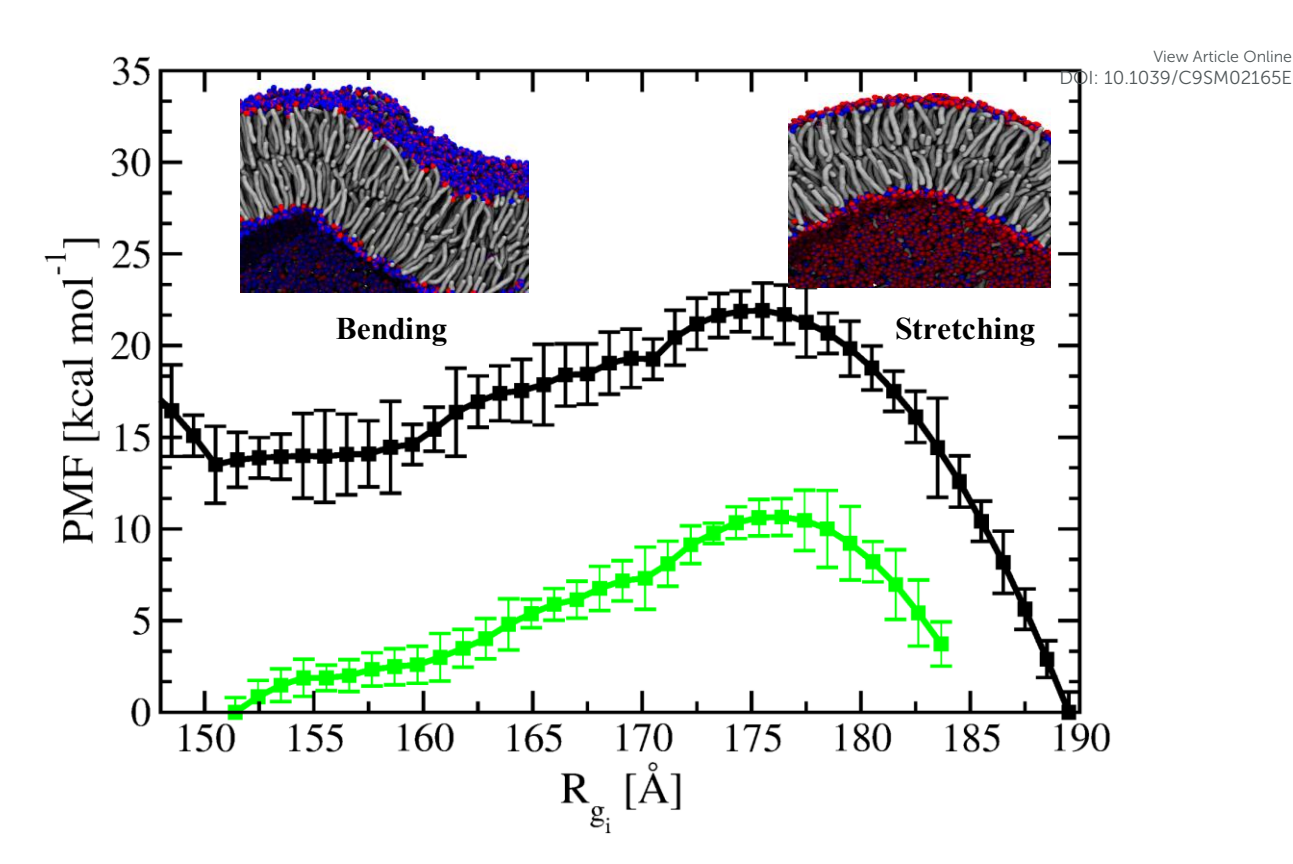


Fig. 8. Potential of mean force (PMF) for the shape change of the polymersome. Here R_{g_i} is the radius of gyration of the inner leaflet. Stretching and bending of the polymersome bilayer due to contraction of inner compartment are clearly evident. These two regimes are separated by a high energy barrier around $^{\sim}$ 20 kcal mol⁻¹. PMF in the presence of only CG water is black, while the PMF in the presence of both CG water and model hydrophobic CG solvent is indicated in green.

solvent, this is the energy cost only due to structural rearrangements of the polymers during shape transformation of the polymersors during shape transformation of the polymersor during solvent is used. The presence of hydropholode solvent speeds up the shape change due to the increased dynamics of the PS chains as demonstrated by the self-intermediate scatteribes function as shown in SI-11.38 and reduces the bending modulus of the PEO-PS membrane as discussed previously. In comparison, in the case that the solvent is mixed CG water and a model hydropholode bead, we find a barrier that decreases by 50% to ~ 10 kcal mol-1. The is qualitatively consistent with the threshold pressure for instability predicted by Ou-Yang and Helfrich 13, and thus the free enerestable barrier, that is predicted to be proportional to the bending rigidity42

CONCLUSIONS

Currently, the molecular picture of how individual polymer chai43 guide the shape transformation of polymersomes is mostly missing. Herein, we perform a systematic analysis of the shape transformation of PEO-PS diblock polymersomes due to reduced volumes and reduced areas of its inner compartment. The presence of two distinct regimes, stretching and bending, of the polymersome membrane are evident. The initial response of the membrane, for experimental observations—an increase in membrane thickness dues to stretching of the PEO-PS polymersome under osmotic pressures stress ²⁴. Furthermore, these two regimes are separated by a high energy barrier of around ~ 20 kcal mol⁻¹. While stretching of individual polymer chains maintains the spherical shape of the polymersome under initial contractions, the bending is responsible

for its final non-spherical geometry. The presence of hydrophobic solvent lowers the barrier free energy for the shape change most likely due to the decreasing bending modulus of the PEO-PS membrane. In the presence of hydrophobic solvent the area elastic modulus also proportionally decreases. These results can help guide experimentalists in the future design of stimuli-responsive polymer vesicles for various applications. The shape of the polymersome is a key factor that regulates interactions of polymersomes with cells^{69,70}. Like red blood cells and disc-like erythrocytes ⁷¹⁻⁷³, the shape of the polymersome is also believed to affect its flow properties ⁷⁴.

SUPPORTING INGORMATION

The shape change of both a small and large polymersome are discussed in SI-1 to SI-12.

Conflicts of interest

"There are no conflicts to declare".

Acknowledgements

S.M.L. acknowledges start-up funding received from College of Staten Island and City University of New York. This work was supported by grants PRF 54235-DNI6, NSF 1506937, and NSF 1750694.

References

ARTICLE Journal Name

	ANTICLL		
1	1.	D. E. Discher and A. Eisenberg, <i>Science</i> , 2002, 297 , 967-97 6 3	28.
2	2.	B. M. Discher, Y. Y. Won, D. S. Ege, J. C. M. Lee, F. S. Bates.	
3		D. E. Discher and D. A. Hammer, <i>Science</i> , 1999, 284 , 114 65	29.
4		1146.	
5	3.	D. E. Discher and F. Ahmed, in <i>Annual Review of Biomedical</i>	
6		Engineering, 2006, vol. 8, pp. 323-341. 68	30.
7	4.	D. Boal and D. H. Boal, <i>Mechanics of the Cell</i> , Cambrid 9	24
8 9	_	University Press, 2012. 70	31.
10	5.	H. Bermudez, D. A. Hammer and D. E. Discher, <i>Langmulf</i> . 2004. 20 . 540-543.	22
11	6.	2004, 20 , 540-543. 72 S. C. Balmert and S. R. Little, <i>Advanced Materials</i> , 2012, 243	32.
12	0.	3757-3778. 74	33.
13	7.	H. C. Shum, J. W. Kim and D. A. Weitz, Journal of the	55.
14	,.	American Chemical Society, 2008, 130 , 9543-9549.	34.
15	8.	D. A. Wilson, R. J. M. Nolte and J. C. M. van Hest, Natura	٠
16	-	Chemistry, 2012, 4 , 268-274. 78	
17	9.	H. L. Che and J. C. M. van Hest, Journal of Material 9	35.
18		<i>Chemistry B,</i> 2016, 4 , 4632-4647.	
19	10.	M. L. Jacobs, M. A. Boyd and N. P. Kamat, Proceedings 81	36.
20		the National Academy of Sciences, 2019.	
21	11.	R. S. M. Rikken, H. Engelkamp, R. J. M. Nolte, J. C. Maan &3	37.
22		C. M. van Hest, D. A. Wilson and P. C. M. Christiane 4.	
23		<i>Nature Communications</i> , 2016, 7 , 12606.	38.
24	12.	U. Seifert, <i>Advances in Physics</i> , 1997, 46 , 13-137.	
25	13.	O. Y. Zhongcan and W. Helfrich, <i>Physical Review Lette</i> 87	39.
26		1987, 59 , 2486-2488.	
27	14.	H. Bermudez, A. K. Brannan, D. A. Hammer, F. S. Bates a	40.
28	4.5	D. E. Discher, <i>Macromolecules</i> , 2002, 35 , 8203-8208. 90	
29 30	15.	D. A. Christian, A. Tian, W. G. Ellenbroek, I. Levental, 91	
31		Rajagopal, P. A. Janmey, A. J. Liu, T. Baumgart and D. 92 Discher, <i>Nature materials</i> , 2009, 8, 843-849.	41.
32	16.	B. M. Discher, H. Bermudez, D. A. Hammer, D. E. Discher, 94	41.
33	10.	Y. Won and F. S. Bates, <i>Journal of Physical Chemistry</i> 95	42.
34		2002, 106 , 2848-2854. 96	72.
35	17.	Z. L. Cheng, D. R. Elias, N. P. Kamat, E. D. Johnston, 97	43.
36		Poloukhtine, V. Popik, D. A. Hammer and A. Tsourk 88	
37		<i>Bioconjugate Chemistry</i> , 2011, 22 , 2021-2029. 99	44.
38	18.	L. F. Zhang and A. Eisenberg, Journal of the Ameril 600	
39		<i>Chemical Society</i> , 1996, 118 , 3168-3181. 101	45.
40	19.	P. L. Soo and A. Eisenberg, Journal of Polymer Science A002	
41		<i>B-Polymer Physics</i> , 2004, 42 , 923-938. 103	46.
42	20.	T. Chidanguro, E. Ghimire, C. H. Liu and Y. C. Simon, Smld04.	
43		2018, 14 . 105	47.
44	21.	K. T. Kim, J. H. Zhu, S. A. Meeuwissen, J. Cornelissen, 1.06	
45		Pochan, R. J. M. Nolte and J. C. M. van Hest, <i>Journal of</i> 169	48.
46	22	American Chemical Society, 2010, 132 , 12522-12524. 108	40
47	22.	L. K. E. A. Abdelmohsen, D. S. Williams, J. Pille, S. G. 0269	49.
48 49		R. S. M. Rikken, D. A. Wilson and J. C. M. van Hest, Jou 1/100 of the American Chemical Society, 2016, 128, 0353, 03511	
50	23.	of the American Chemical Society, 2016, 138, 9353-935611 Y. Men, W. Li, GJ. Janssen, R. S. M. Rikken and D112	
51	23.	Wilson, <i>Nano Letters</i> , 2018, 18 , 2081-2085.	
52	24.	S. A. Meeuwissen, K. T. Kim, Y. Chen, D. J. Pochan and 114	
53		M. van Hest, Angewandte Chemie International Editabs	50.
54		2011, 50 , 7070-7073.	20.
55	25.	R. Salva, JF. Le Meins, O. Sandre, A. Brûlet, M. Schmut 1,17	51.
56		Guenoun and S. Lecommandoux, ACS Nano, 2013, 7, 92988	
57		9311. 119	52.
58	26.	U. Seifert, K. Berndl and R. Lipowsky, <i>Physical Review</i> 20	
59		1991, 44 , 1182-1202.	53.
60	27.	V. Ortiz, S. O. Nielsen, D. E. Discher, M. L. Klein, R. Lipows 22	
61		and J. Shillcock, Journal of Physical Chemistry B, 2005, 1023	54.
62		17708-17714. 124	

Published on 04 March 2020. Downloaded by RSC Internal on 3/5/2020 10:14:04 AM

- X. J. Li, I. V. Pivkin, H. J. Liang and G. E_{vie} Karniadakis, *Macromolecules*, 2009, **42**, 3195-3200.10.1039/C9SM02165E M. Muller and J. J. de Pablo, in *Annual Review of Materials Research, Vol 43*, Annual Reviews, Palo Alto, 2013, vol. 43, pp. 1-34.
- V. A. Harmandaris, N. P. Adhikari, N. F. A. van der Vegt and K. Kremer, *Macromolecules*, 2006, **39**, 6708-6719.
- F. Varnik, J. Baschnagel and K. Binder, *Physical Review E*, 2002, **65**.
- K. Yoshimoto, T. S. Jain, K. V. Workum, P. F. Nealey and J. J. de Pablo, *Physical Review Letters*, 2004, **93**.
- G. Milano and F. Muller-Plathe, *Journal of Physical Chemistry B*, 2005, **109**, 18609-18619.
- H. A. Harimi-Varzaneh, N. F. A. van der Vegt, F. Mueller Plathe and P. Carbone, *ChemPhysChem*, 2012, **Advance Article**.
- G. Rossi, L. Monticelli, S. R. Puisto, I. Vattulainen and T. Ala-Nissila, *Soft Matter*, 2011, **7**, 698-708.
- W. Shinoda, R. DeVane and M. L. Klein, *Molecular Simulation*, 2007, **33**, 27-36.
- M. Drenscko and S. M. Loverde, *Molecular Simulation*, 2017, **43**, 234-241.
- K. Chakraborty, K. Vijayan, A. E. X. Brown, D. E. Discher and S. M. Loverde, *Soft Matter*, 2018, **14**, 4194-4203.
- G. M. Torrie and J. P. Valleau, *Journal of Computational Physics*, 1977, **23**, 187-199.
- G. Fiorin, M. L. Klein, R. DeVane and W. Shinoda, in *Hierarchical Macromolecular Structures: 60 Years after the Staudinger Nobel Prize II*, Springer International Publishing, 2013, pp. 93-107.
- W. Shinoda, R. DeVane and M. L. Klein, *Current Opinion in Structural Biology*, 2012, **22**, 175-186.
 - S. C. L. Kamerlin, S. Vicatos, A. Dryga and A. Warshel, Annual Review of Physical Chemistry, 2011, **62**, 41-64.
 - S. M. Loverde, M. L. Klein and D. E. Discher, *Advanced materials*, 2012, **24**, 3823-3830.
 - W. Shinoda, D. E. Discher, M. L. Klein and S. M. Loverde, Soft Matter, 2013, **9**, 11549-11556.
 - S. M. Loverde, V. Ortiz, R. D. Kamien, M. L. Klein and D. E. Discher, *Soft Matter*, 2010, **6**, 1419-1425.
 - W. Shinoda, R. DeVane and M. L. Klein, *Molecular Simulation*, 2007, **33**, 27-36.
- W. Shinoda, R. DeVane and M. L. Klein, *Soft Matter*, 2008, **4**, 2454-2462.
 - X. He, W. Shinoda, R. DeVane and M. L. Klein, *Molecular Physics*, 2010, **108**, 2007-2020.
 - V. Percec, D. A. Wilson, P. Leowanawat, C. J. Wilson, A. D. Hughes, M. S. Kaucher, D. A. Hammer, D. H. Levine, A. J. Kim, F. S. Bates, K. P. Davis, T. P. Lodge, M. L. Klein, R. H. DeVane, E. Aqad, B. M. Rosen, A. O. Argintaru, M. J. Sienkowska, K. Rissanen, S. Nummelin and J. Ropponen, *Science*, 2010, **328**, 1009-1014.
 - S. Plimpton, *Journal of Computational Physics*, 1995, **117**, 1-19.
 - S. E. Feller, Y. Zhang, R. W. Pastor and B. R. Brooks, *The Journal of Chemical Physics*, 1995, **103**, 4613-4621.
 - W. Shinoda, M. Shiga and M. Mikami, *Physical Review B*, 2004, **69**.
 - M. Parrinello and A. Rahman, Journal of Applied Physics, 1981, 52, 7182-7190.
 - G. J. Martyna, D. J. Tobias and M. L. Klein, *Journal of Chemical Physics*, 1994, **101**, 4177-4189.

Published on 04 March 2020. Downloaded by RSC Internal on 3/5/2020 10:14:04 AM.

33

34

35

36

37

38

39

45

View Article Online

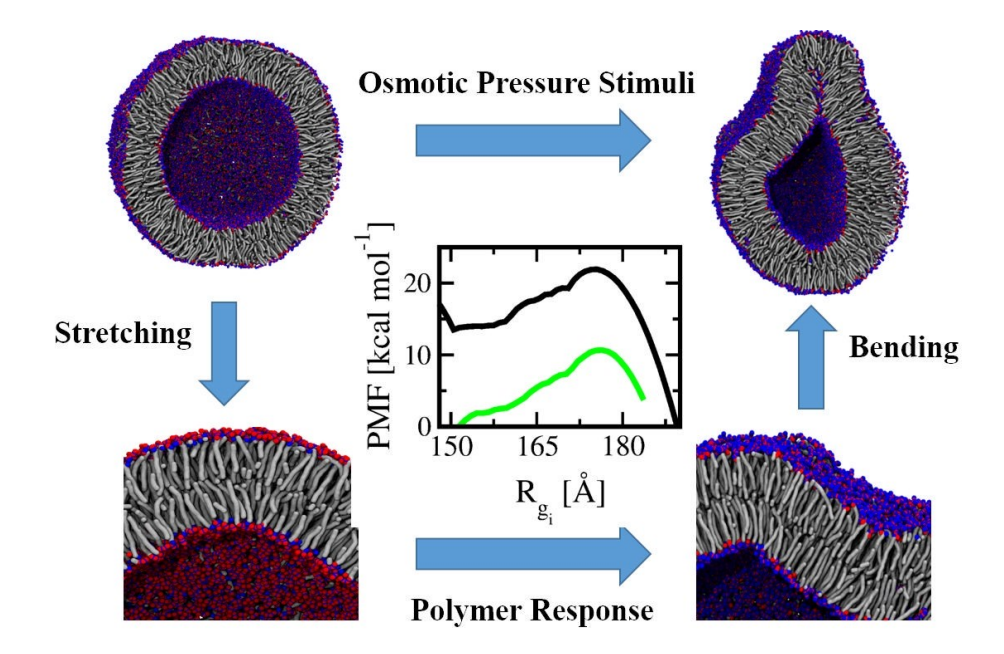
DOI: 10.1039/C9SM02165E

Journal Name ARTICLE

1 55. J. Kästner, Wiley Interdisciplinary Reviews: Computational Molecular Science, 2011, 1, 932-942.

- 3 56. F. Zhu and G. Hummer, Journal of Computational Chemistry, 2012, **33**, 453-465.
- 5 57. S. Kumar, J. M. Rosenberg, D. Bouzida, R. H. Swendsen and
 P. A. Kollman, *Journal of Computational Chemistry*, 1992,
 13, 1011-1021.
- 8 58. K. Chakraborty, M. Kang and S. M. Loverde, *Journal of Physical Chemistry B*, 2018, **122**, 11827-11840
- 10 59. H. C. a. A. Z. Panagiotopoulos, *Langmuir*, 2019.
- 11 60. G. Srinivas, D. E. Discher and M. L. Klein, *Nature materials*,
 2004, 3, 638-644.
- 13 61. V. Ortiz, S. O. Nielsen, D. E. Discher, M. L. Klein, R. Lipowsky
 14 and J. Shillcock, *The journal of physical chemistry*, 2005,
 15 109, 17708-17714.
- 16 62. D. A. Grillo, J. M. R. Albano, E. E. Mocskos, J. C. Facelli, M.
 17 Pickholz and M. B. Ferraro, *The Journal of Chemical Physics*,
 2017, 146, 244904.
- 19 63. P. Fromherz, *Chemical Physics Letters*, 1983, **94**, 259-266.
- 20 64. W. Shinoda, T. Nakamura and S. O. Nielsen, *Soft Matter*,
 21 2011, 7, 9012-9020.
- Y. Kim, K. S. Kim, K. L. Kounovsky, R. Chang, G. Y. Jung, J. J.
 dePablo, K. Jo and D. C. Schwartz, *Lab on a Chip*, 2011, 11, 1721-1729.
- 25 66. M. C. Watson, E. S. Penev, P. M. Welch and F. L. H. Brown,
 Journal of Chemical Physics, 2011, 135.
- S. Kawamoto, T. Nakamura, S. O. Nielsen and W. Shinoda,
 The Journal of Chemical Physics, 2013, 139, 034108.
- M. C. Watson, E. G. Brandt, P. M. Welch and F. L. H. Brown, *Physical Review Letters*, 2012, 109, 028102.
- 31 69. J. L. Perry, K. P. Herlihy, M. E. Napier and J. M. DeSimone,
 32 Accounts of Chemical Research, 2011, 44, 990-998.
 - P. Kolhar, A. C. Anselmo, V. Gupta, K. Pant, B. Prabhakarpandian, E. Ruoslahti and S. Mitragotri, Proceedings of the National Academy of Sciences, 2013, 110, 10753.
 - 71. N. Doshi, A. S. Zahr, S. Bhaskar, J. Lahann and S. Mitragotri, *Proceedings of the National Academy of Sciences*, 2009, **106**, 21495.
- 40 72. H.-Y. Chang, Y.-J. Sheng and H.-K. Tsao, *Soft Matter*, 2014, 41 **10**, 6373-6381.
- 42 73. C. Uzoigwe, Medical Hypotheses, 2006, 67, 1159-1163.
- 43 74. J. R. Rothenbuhler, J.-R. Huang, B. A. DiDonna, A. J. Levine and T. G. Mason, *Soft Matter*, 2009, **5**, 3639-3645.

This journal is © The Royal Society of Chemistry 20xx



204x125mm (150 x 150 DPI)

Published on 04 March 2020. Downloaded by RSC Internal on 3/5/2020 10:14:04 AM.